PLOS ONE

RESEARCH ARTICLE

Fluid Forces Enhance the Performance of an Aspirant Leader in Self-Organized Living Groups

Alessandro De Rosis*

Department of Agricultural Sciences, University of Bologna, Bologna, Italy

*alessandro.derosis@unibo.it

Abstract

In this paper, the performance of an individual aiming at guiding a self-organized group is numerically investigated. A collective behavioural model is adopted, accounting for the mutual repulsion, attraction and orientation experienced by the individuals. Moreover, these represent a set of solid particles which are supposed to be immersed in a fictitious viscous fluid. In particular, the lattice Boltzmann and Immersed boundary methods are used to predict the fluid dynamics, whereas the effect of the hydrodynamic forces on particles is accounted for by solving the equation of the solid motion through the time discontinuous Galerkin scheme. Numerical simulations are carried out by involving the individuals in a dichotomous process. On the one hand, an aspirant leader (AL) additional individual is added to the system. AL is forced to move along a prescribed direction which intersects the group. On the other hand, these tend to depart from an obstacle represented by a rotating lamina which is placed in the fluid domain. A numerical campaign is carried out by varying the fluid viscosity and, as a consequence, the hydrodynamic field. Moreover, scenarios characterized by different values of the size of the group are investigated. In order to estimate the AL's performance, a proper parameter is introduced, depending on the number of individuals following AL. Present findings show that the sole collective behavioural equations are insufficient to predict the AL's performance, since the motion is drastically affected by the presence of the surrounding fluid. With respect to the existing literature, the proposed numerical model is enriched by accounting for the presence of the encompassing fluid, thus computing the hydrodynamic forces arising when the individuals move.

CrossMark
click for updates

OPEN ACCESS

Citation: De Rosis A (2014) Fluid Forces Enhance the Performance of an Aspirant Leader in Self-Organized Living Groups. PLoS ONE 9(12): e114687. doi:10.1371/journal.pone.0114687

Editor: Francesco Pappalardo, University of Catania, Italy

Received: September 4, 2014

Accepted: November 12, 2014

Published: December 15, 2014

Copyright: © 2014 Alessandro De Rosis. This is an open-access article distributed under the terms of the Creative Commons Attribution License, which permits unrestricted use, distribution, and reproduction in any medium, provided the original author and source are credited.

Data Availability: The authors confirm that all data underlying the findings are fully available without restriction. All data files are contained within the paper.

Funding: The author has no support or funding to report.

Competing Interests: The author has declared that no competing interests exist.

Introduction

Social interactions involve the decision processes emerging in many animal groups, such as flocks of birds, schools of fishes or swarms of insects [1–5]. In particular, these organized groups routinely perform several decisions which are often remarkably crucial to enhance their survival chances. In fact, a particular kind of benefit is identified in predatory avoidance in schools of fishes [6–11], consisting of evasive manoeuvres confusing the attacking predator [12]. On the other hand, increasing attention has been devoted to the leader identification process [13–18]. A better understanding of such phenomenon can have a huge impact in a lot of applications. Among these, one of the most interesting is related to the design of a drone which can guide the real fishes towards a prescribed direction. For example, in [19] the response of fishes has been widely investigated by varying several morphological characteristics of the robot, showing that its size and color pattern strongly influence fish preferences. In [20], the interactions between two social fish species, zebrafish and mosquitofish, and a zebrafish-like robot have been discussed, showing that the robot tends to attract the zebrafishes, whereas the others are repulsed. Intriguing findings have been highlighted in [21], where it has been found that the biomimetic locomotion can alter fish preferences, since the tail beating attracts more the fishes towards the robot rather than when it is motionless. In [22], scenarios characterized by different beating frequencies have been dissected, showing that fish preferences are strongly influenced by the motion pattern. In [23], experiments in a water tunnel have been performed, elucidating the influence of both robot color and beating frequency on fish behaviour. These findings corroborate biological evidence that salient aspects of fish schooling benefit from the presence of group leaders [17, 18]. Several works [24–28] showed how the number of informed individuals affects the decision-making and leader identification processes for the uninformed ones. Moreover, these results can be used to design artificial leaders that can regulate collective behaviour. In order to perform effective and accurate predictions of the behaviour of a group of individuals, a lot of numerical models have been developed [29–34]. Such methods are based on metric [15, 35, 36] or topological [37–41] collective behavioural rules, which describe the mutual interaction in terms of reciprocal repulsion, attraction and orientation tendencies.

In this paper, beside the uniquely *social* approaches, the prediction of the leader identification and decision making processes emerging in a set of self-organized individuals is enriched by accounting for the presence of the encompassing fluid. Specifically, the lattice Boltzmann (LB) method is adopted to predict the fluid dynamics [42–44]. The LB method has been preferred to standard Navier-Stokes based solvers due to its algorithmical simplicity and computational efficiency, especially if force computations are involved in the numerical simulations, as in the present paper. In order to account for the presence of an immersed solid body (i.e. the individuals), the Immersed boundary (IB) method [45–47] is employed. The choice of the IB method over the well-consolidated interpolated bounce-back rule [48–51] is motivated by its superior properties in terms of numerical stability

and by its high accuracy and convergence features, as recently demonstrated by the author [52]. Moreover, the combination of the LB and IB methods leads to the implementation of a quite general algorithm [53], which has been successfully used by the author in a lot of practical applications, including flapping wing dynamics [54, 55], shallow waters [56], multiphase flows [57], and even non-Newtonian fluid [58], among the others. Once fluid forces have been computed, the solid dynamics, i.e. the one involving the individuals, is computed through the time discontinuous Galerkin (TDG) scheme, which is known to possess high properties in terms of stability, convergence and accuracy [59, 60]. On the other hand, the collective behavioural model á la Couzin [15, 35] is adopted to compute the space-time evolution of the group. An additional aspirant leader (AL) individual is added to the group and it is forced to move towards a prescribed direction. During its motion, it meets the group and a certain portion of the individuals follows it. The AL's performance are assessed by proposing a proper parameter, as discussed in the following. Scenarios characterized by different values of the fluid viscosity are investigated. Moreover, the effect of the size of the group is dissected too. Numerical findings show that the purely behavioural modelling is insufficient to predict the AL's performance if it is immersed in a fluid, since the fluid dynamics plays a crucial role. It is worth to notice that the novelty of the present work with respect to the existing literature is represented by the insertion and the investigation of the dependence of the leader identification and decision making processes on the encompassing hydrodynamic field.

The rest of the paper is organized as follows. In the Methods section, the adopted numerical methods are recalled. In the Results and Discussion section, findings from a numerical campaign are presented and discussed. Finally, some conclusions are drawn in the Conclusion section.

Methods

Here, the adopted numerical methods are briefly recalled and the proposed algorithm of computation is presented.

Collective behavioural model

According to [15], the spatial position $\mathbf{X}^i$ of the generic individual i is updated in time t as follows

$$\mathbf{X}^i(t+\Delta t)=\mathbf{X}^i(t)+\mathbf{V}^i(t)s\Delta t, \tag{1}$$

where $\Delta t=1$ is the time step, $s=0.01$ is the cruising speed and $\mathbf{V}^i$ is the normalized velocity vector. Specifically, such quantity is computed as the summation of three contributions, i.e.

$$\mathbf{V}^i(t)=\mathbf{V}^i_r(t)+\mathbf{V}^i_{a,o}(t)+\mathbf{V}^i_{AL}(t), \tag{2}$$

where

$$\mathbf{V}_r^i(t) = -\sum_{k\neq i} \frac{\mathbf{X}^k(t)-\mathbf{X}^i(t)}{|\mathbf{X}^k(t)-\mathbf{X}^i(t)|}, \quad \text{if} \quad |\mathbf{X}^k(t)-\mathbf{X}^i(t)| \leq r_1, \tag{3}$$

$$\mathbf{V}_{a,o}^i(t) = w_a \sum_{k\neq i} \frac{\mathbf{X}^k(t)-\mathbf{X}^i(t)}{|\mathbf{X}^k(t)-\mathbf{X}^i(t)|} + w_o \sum_k \frac{\mathbf{V}^k(t)}{|\mathbf{V}^k(t)|}, \quad \text{if} \quad r_1 < |\mathbf{X}^k(t)-\mathbf{X}^i(t)| \leq r_2, \tag{4}$$

$$\mathbf{V}_{AL}^i(t) = \frac{\mathbf{X}^{AL}(t)-\mathbf{X}^i(t)}{|\mathbf{X}^{AL}(t)-\mathbf{X}^i(t)|}, \quad \text{if} \quad r_1 < |\mathbf{X}^{AL}(t)-\mathbf{X}^i(t)| \leq r_3. \tag{5}$$

Making reference to Fig. 1, the first equation accounts for the mutual repulsion and it is valid in a circular area of radius r_1. If the individual i identifies another individual, namely k, it moves in order to avoid collisions. The second one is the attraction-orientation equation: the individual i tends to get attracted and aligned with respect to individuals found in the area of radius $r_2 - r_1$. Attraction and orientation are weighted through proper coefficients, namely $w_a = 0.5$ and $w_o = 0.5$, respectively. The third one is proposed by the author in order to account for the AL's influence. Specifically, AL is idealized as an additional individual which is located at the position $\mathbf{X}^{AL}$. The generic individual i undergoes AL-induced attraction or orientation if the aspirant leader is detected in an area of radius $r_3 - r_1$. Notice that the area where the individual i senses the AL's influence is intentionally set larger than the one of radius r_2, i.e. $r_3 > r_2$. In fact, AL can be designed in order to be more persuasive than a real living individual, as discussed in the previous section. The individual i possesses a blind conic zone of angle $\beta = 20^\circ$ that is located in the direction opposite to the motion. Individuals which are detected here are completely neglected. Moreover, AL is forced to move towards the prescribed fixed point $\mathbf{X}^p$. Therefore, the AL's velocity vector is computed as

$$\mathbf{V}^{AL}(t) = \frac{\mathbf{X}^p - \mathbf{X}^{AL}(t)}{|\mathbf{X}^p - \mathbf{X}^{AL}(t)|}. \tag{6}$$

Concerning the presence of an obstacle (e.g. a rotating lamina), it is identified as an additional set of individuals with respect to the group is repulsed, whereas the attraction-orientation rule is neglected. Such tendency is enforced even for AL.

The LB-IB-TDG strategy

The two-dimensional Bhatnagar-Gross-Krook [61] equation is solved on an Eulerian fixed square grid (see Fig. 2) where the particle distribution functions f_j are forced to move along prescribed directions with velocities $\mathbf{e}_j$ connecting the

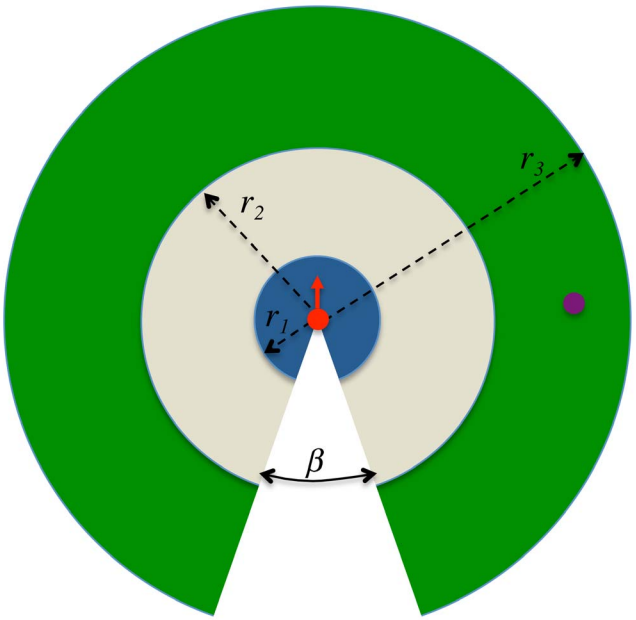

Fig. 1. Schematic representation of the adopted behavioural model. The generic individual i (red circle) moves along a direction (red arrow). Repulsion and attraction-orientation circular areas have radius $r_1 = 5$ and $r_2 = 7$, respectively. If AL (magenta circle) is detected in the area of radius $r_3 - r_1 = 5$, it exerts its influence on the individual i. All the rules are neglected in the blind zone described by the angle β.

doi:10.1371/journal.pone.0114687.g001

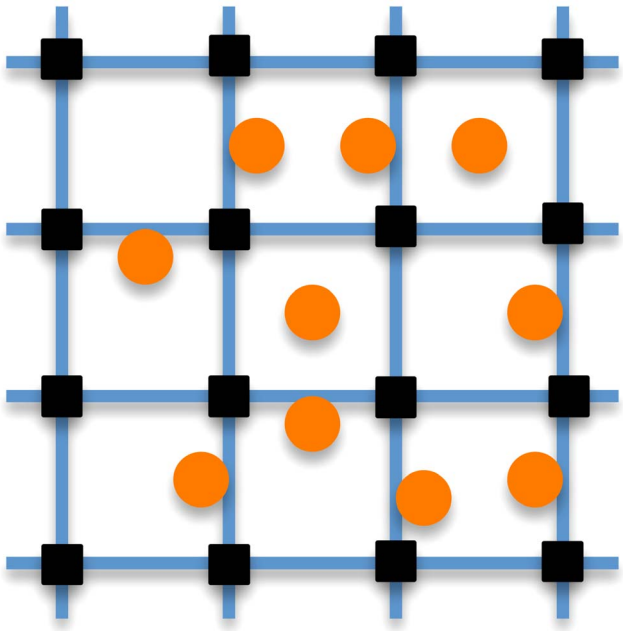

Fig. 2. A set of particles (orange circles) are immersed in an Eulerian fixed square grid (blue lines). The black squares represent the lattice nodes.

doi:10.1371/journal.pone.0114687.g002

lattice nodes (black squares). This equation reads as follows

$$f_j(\mathbf{x}+\mathbf{e}_j\Delta t,t+\Delta t)=f_j(\mathbf{x},t)+\frac{1}{\tau}[f_j^{eq}(\mathbf{x},t)-f_j(\mathbf{x},t)]+3q_j\mathbf{e}_j\cdot\boldsymbol{g}(\mathbf{x},t), \tag{7}$$

where $\mathbf{x}$ is the position, f_j^{eq} are the so-called equilibrium distribution functions [43], q_j is a set of nine weights depending on the adopted LB D2Q9 model [44] and $\boldsymbol{g}(\mathbf{x},t)$ is a correction term. Given the relaxation time τ, the fluid viscosity can be computed as $\nu=\left(\tau-\frac{1}{2}\right)c_s^2$, $c_s=1/\sqrt{3}$ being the lattice sound speed, [44]. In the LB method, the macroscopic fluid density ρ and the flow velocities $\mathbf{v}$ are easily computed as:

$$\rho(\mathbf{x},t)=\sum_j f_j(\mathbf{x},t), \qquad \mathbf{v}(\mathbf{x},t)=\frac{\sum_j f_j(\mathbf{x},t)\mathbf{e}_j}{\sum_j f_j(\mathbf{x},t)}, \tag{8}$$

respectively.

In order to account for the presence of an immersed body (orange circles) in the fluid lattice background at the position $\mathbf{X}^i$, the Immersed Boundary method [45, 46] is adopted. The IB method has been implemented according to an implicit velocity-correction based procedure [47, 52, 53] which iterates in order to enforce the no-slip condition at the fluid-solid interface. A correction term $\boldsymbol{g}(\mathbf{x},t)$ is calculated and it is used in the right-hand side of Equation 7. The computation of such term is highly important, since it leads rapidly to the force acting upon the immersed body as follows

$$\boldsymbol{F}^i=-\sum_{\mathbf{x}}\boldsymbol{g}(\mathbf{x})W(\mathbf{x}-\mathbf{X}^i), \tag{9}$$

W being a kernel support [46]. Notice that the individuals and AL are idealized as circular objects of radius $r=0.016$.

In order to compute the time- and force-dependent displacements $\boldsymbol{u}^i(t)$ of an immersed body, i.e. the generic individual i, the equation of the rigid solid motion is solved, that is

$$m\ddot{\boldsymbol{u}}^i(t)=\boldsymbol{F}^i(t), \tag{10}$$

where $m=5\times10^4$ is the mass of the individuals, which is kept identical for the whole members of the system, and the time derivatives are indicated by superimposed dots. Equation 10 is numerically resolved by adopting the TDG algorithm. The interested reader can refer to [59] for further details about such time integration scheme. The author remarks that the strategy combining the LB, IB and TDG methods for solving fluid-structure interaction problems has already been widely validated [53]. In order to perform the conversion from lattice units to physical ones, the author selects a length scale factor $S_l=1\times10^{-4}\,\mathrm{m}$, a velocity scale factor $S_v=1\times10^{-2}\,\mathrm{m/s}$ and a density scale factor $S_\rho=1\times10^3\,\mathrm{kg/m^3}$.

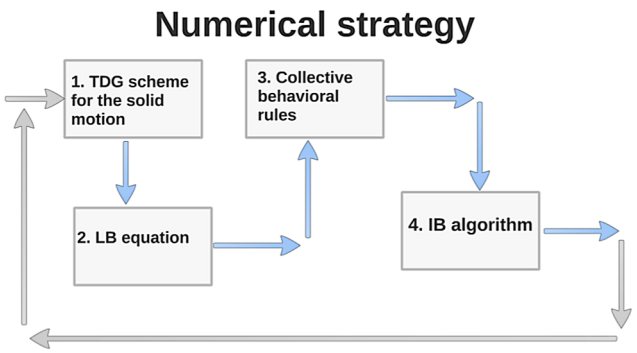

Fig. 3. Sketch of the algorithm of computation.

doi:10.1371/journal.pone.0114687.g003

Algorithm of computation

The above mentioned numerical methods are combined in a proper strategy, consisting of an algorithmical sequence of actions which are sketched in Fig. 3. After assigning the initial values of the density and flow velocity, together with the initial position and velocity of the immersed bodies, the loop spanning the prescribed time range starts. In particular, the first action consists of solving the equation of the solid motion, i.e. Equation 10, for each individual. Thus, the positions and velocities of the individuals are updated. Notice that such action needs the displacements and velocities of the previous time step, together with the fluid forces. Secondly, the LB equation is solved by neglecting the last term in the right-hand side and the fluid macroscopic variables (i.e. ρ and $\mathbf{v}$) are computed. Thirdly, the position of the individuals is updated by solving Equation 1. Fourthly, the term $3q_j\boldsymbol{e}_j\cdot\boldsymbol{g}(\mathbf{x},t)$ is computed through the implicit IB algorithm [52] and it is used to correct the particle distribution functions f_j and the flow velocity $\mathbf{v}$. In order to advance in time, the algorithm repeats these tasks by using as initial conditions the displacements and velocities of the previous time step. The algorithm of computation is summarized in Table 1.

Results and Discussion

The problem set-up is sketched in Fig. 4. In particular, the fluid domain consists of $W=200$ and $H=100$ lattice nodes. AL is placed at $(x_1,x_2)=(0,50)$. It is represented by the magenta point and it is forced to move towards the point $\mathbf{X}^p=(200,50)$. A lamina (black line), whose top-most point is fixed at the center of the fluid domain, undergoes a harmonic rotation, that is $\theta(t)=\Delta\theta\cos\left(\frac{2\pi t}{T}\right)$, where θ is the rotation angle, $\Delta\theta=\pi/4$ is the maximum angle and $T=2000$ is the period of oscillation. The lamina is idealized by $L=5$ lattice nodes. The white line represents the initial position of the group. Notice that the top-most one is placed at $(x_1,x_2)=(50,55)$ and the bottom-most one at $(x_1,x_2)=(50,45)$. Depending on the number of individuals forming the group, the initial reciprocal spacing varies

Table 1. Flow chart of the algorithm of computation.

0 - assign initial conditions and then start the loop on the time span;
1 - solve the equation of the solid motion for each individual,
$m\ddot{\mathbf{u}}^i(t)=\mathbf{F}^i(t)$;
2 - solve LB equation without the correction IB term,
$f_j(\mathbf{x}+\Delta t\,\mathbf{e}_j,t+\Delta t)=f_j(\mathbf{x},t)+\frac{1}{\tau}[f_j^{eq}(\mathbf{x},t)-f_j(\mathbf{x},t)]$;
3 - update the position of the individuals,
$\mathbf{X}^i(t+\Delta t)=\mathbf{X}^i(t)+\mathbf{V}^i(t)s\Delta t$;
4 - perform the IB implicit algorithm, correct f_j and $\mathbf{v}$ and advance in time going to step 1.

doi:10.1371/journal.pone.0114687.t001

accordingly. All the simulations are characterized by a low Mach number, $\mathcal{M}a=s/c_s=0.017$, thus drastically annihilating deleterious compressibility effects which can affect the LB equation [44]. Scenarios characterized by progressively larger sizes of the group, N, are investigated, i.e. $N=5,\ 10,\ 20,\ 40$. For a given value of N, the effect of the fluid forces is elucidated by adopting different values of the fluid viscosity v, i.e. $v=0.01\bar{6},\ 0.08\bar{3},\ 0.1\bar{6}$. Findings are compared to a scenario characterized by the absence of the hydrodynamics. All the numerical simulations stop after 20 000 time steps.

In Fig. 5, the time evolution of the distance between the group centroid and the AL's position is depicted. Specifically, each graph refers to a value of v and four curves are reported, corresponding to the spectrum of the values of N. The scenario neglecting the fluid presence is reported too. As it is possible to observe, graphs show a common pattern until $t\sim 4500$, which represents the time employed by AL to reach the group. Therefore, the distance tends to reduce. In the remaining part of the considered time span, the scenario characterized by the absence of the hydrodynamics is drastically different with respect to the other ones. In particular, if the fluid is neglected the distance tends to grow in time, independently from the considered value of N. This means that AL passes through

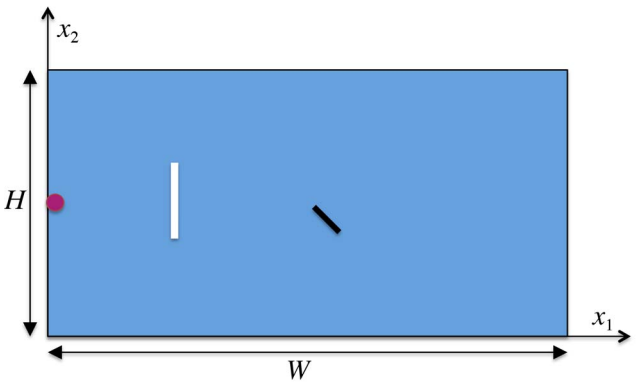

Fig. 4. Sketch of the problem set-up. The individuals are represented by the white line. A lamina, whose top-most point is fixed at the center of the fluid domain, rotates harmonically. AL is placed at $(x_1,x_2)=(0,50)$ and it is enforced to move strictly rightward.

doi:10.1371/journal.pone.0114687.g004

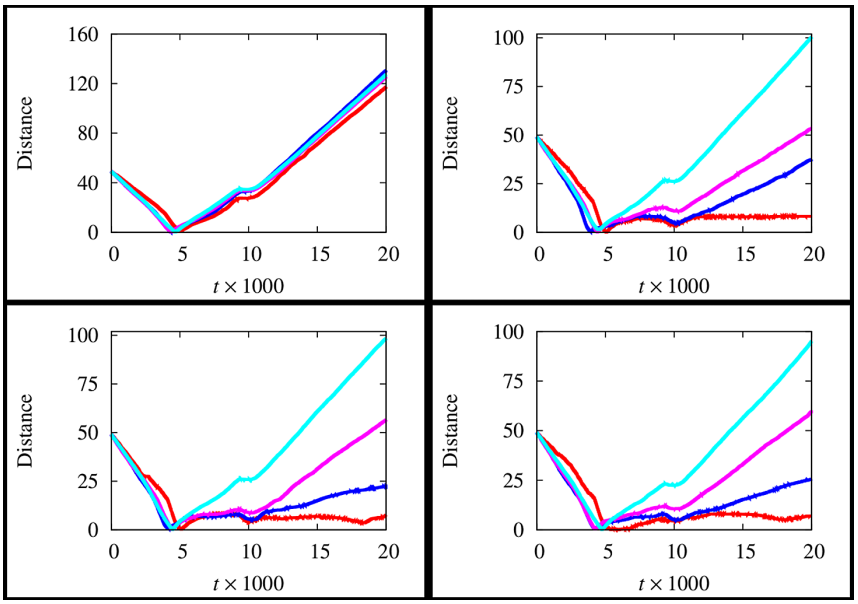

Fig. 5. Time evolution of the distance between the group centroid and the position of AL for different values of v, i.e. $v=0.016$ (top right panel), $v=0.083$ (bottom left panel), $v=0.16$ (bottom right panel), at $N=5$ (red), 10 (blue), 20 (magenta), 40 (cyan). The scenario neglecting the fluid presence is reported in the top left panel.

doi:10.1371/journal.pone.0114687.g005

the group and it is unable to successfully attract the individuals. On the other hand, as v grows, such distance assumes lower values, thus allowing to assess that the group tends to get closer to AL. Therefore, the fluid presence plays a remarkably important role in the AL's performance. Such results are confirmed in Fig. 6, where each graph refers to a value of N and four curves are reported, corresponding to the spectrum values of v. Specifically, it is worth to notice that the red curve, corresponding to the absence of the hydrodynamics, is considerably far from the curves representing the remaining configurations. Moreover, the effect of the size of the group is elucidated. In particular, notice that as N increases, the distance becomes larger. This means that, for a given value of v, AL is more attractive as N decreases. This suggests that AL is more effective for groups characterized by small sizes. The number of individuals following AL is reported in Table 2 for the all above mentioned scenarios. The author quantifies the improvement in the AL's performance by defining the hydrodynamic effect HE, that is

$$HE = \frac{N^h - N^{n,h}}{N}, \tag{11}$$

where N^h and $N^{n,h}$ represent the number of individuals following AL in scenarios characterized by the presence and the absence of the hydrodynamics, respectively. In Fig. 7, the hydrodynamic effect is depicted. As above stated, the fluid-induced enhancement of the AL's performance is more marked as N decreases.

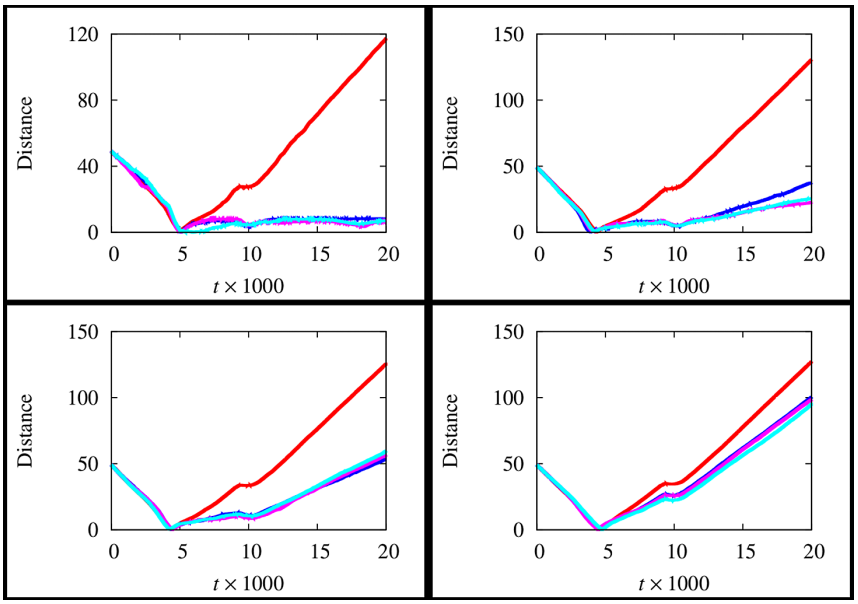

Fig. 6. Time evolution of the distance between the group centroid and the position of AL for different values of N. i.e. $N=5$ (top left panel), $N=10$ (top right panel), $N=20$ (bottom left panel), $N=40$ (bottom right panel), at $v=0.016$ (blue), $0.08\bar{3}$ (magenta), $0.1\bar{6}$ (cyan). The scenario neglecting the fluid presence is denoted by the red curve.

doi:10.1371/journal.pone.0114687.g006

A deeper investigation on the space-time evolution of the group is carried out by sketching the spatial configuration of the individuals at $t=20000$ for the above discussed scenarios, thus highlighting the fragmentation of the group. Notice that it is induced by both AL and the lamina. In particular, in Fig. 8 scenarios characterized by the absence of the hydrodynamics are reported. As it is possible to observe, the group is progressively more elongated as N grows, due to the AL's transit. In particular, notice that at $N=10$ two individuals separate from the group. At $N=20$, four individuals arrive close to the lamina, whose presence stops these. In this configuration, it is intriguing to notice that an individual tends to follow AL, but when it reaches the lamina, it is obstructed. Then, it loses the route, thus moving in an a priori unpredictable direction. At $N=40$, six individuals stall close to the lamina, whereas the remaining part falls behind, showing a certain level of elongation. Scenarios characterized by $v=0.01\bar{6}$ are depicted in Fig. 9. At

Table 2. Number of individuals following AL for different values of v and N.

	$N=5$	$N=10$	$N=20$	$N=40$
No fluid	**0**	**0**	**0**	**0**
$v=0.01\bar{6}$	5	6	11	10
$v=0.08\bar{3}$	5	8	10	11
$v=0.1\bar{6}$	5	8	10	7

The scenario neglecting the fluid presence is reported too.

doi:10.1371/journal.pone.0114687.t002

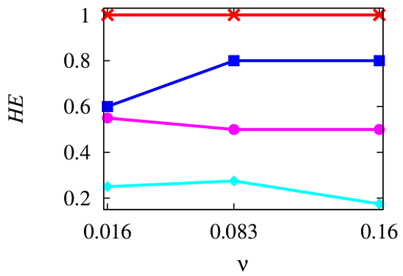

Fig. 7. The hydrodynamic effect, HE, is reported for different values of v, i.e. $v = 0.01\bar{6}, 0.08\bar{3}, 0.1\bar{6}$, at $N = 5$ (red), 10 (blue), 20 (magenta), 40 (cyan).

doi:10.1371/journal.pone.0114687.g007

$N = 5$, AL successfully attracts and guides the whole group. Such results are partially achieved at $N = 10$, where four individuals stop their motion close to the lamina. At $N = 20$, nine individuals miss the goal. Notice that two subgroups can be identified within these nine individuals: the former is represented by the four right-most ones which are obstructed by the lamina, the latter is composed by the remaining ones, which fall behind and then these tend to merge. At $N = 40$, ten individuals are guided, eleven stall close to the lamina and the remaining nineteen are substantially torpid with respect to the AL's transit. If $v = 0.08\bar{3}$ is considered (see Fig. 10), results discussed for the previous scenario are substantially confirmed, even if AL appears to be slightly more persuasive. Finally, it is interesting to notice that at $v = 0.1\bar{6}$ the splitting effect is more marked. Specifically, at $N = 20$ and $N = 40$ three and four well distinct subgroups arise,

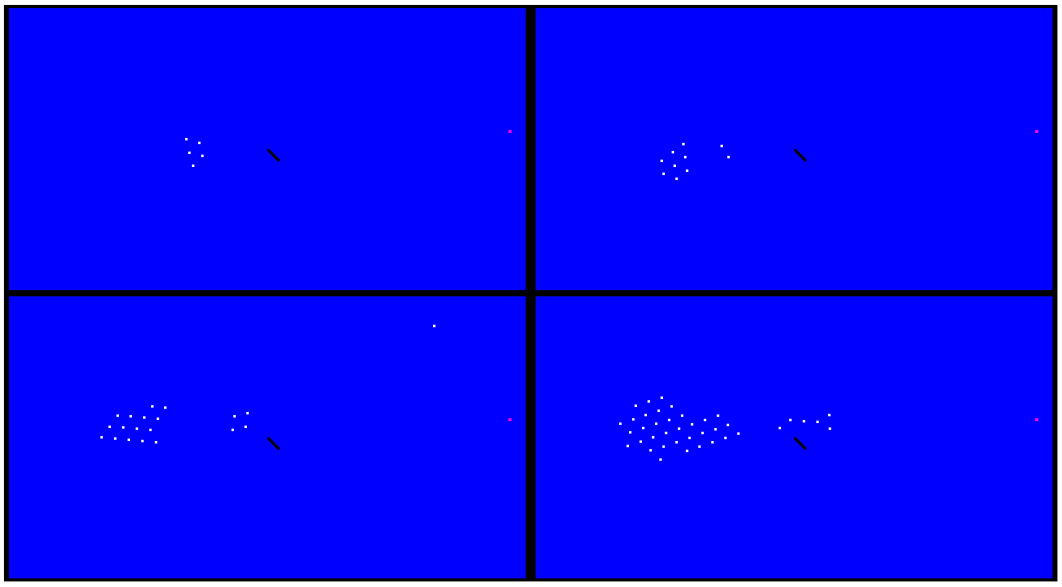

Fig. 8. Absence of the hydrodynamics. Spatial configuration of the individuals (white) for different values of N, i.e. $N = 5$ (top left panel), $N = 10$ (top right panel), $N = 20$ (bottom left panel), $N = 40$ (bottom right panel). AL is coloured by magenta, while the rotating lamina is represented by the black solid line.

doi:10.1371/journal.pone.0114687.g008

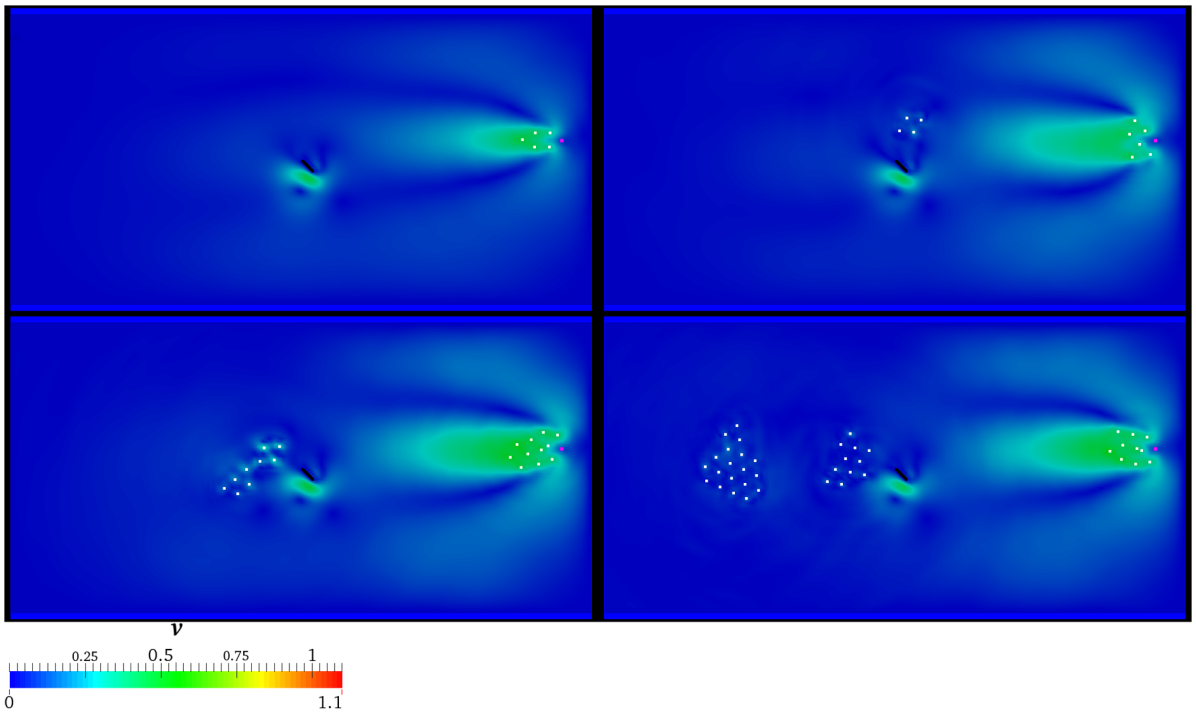

Fig. 9. Presence of the hydrodynamics: $v = 0.01\bar{6}$. Velocity field and spatial configuration of the individuals (white) for different values of N, i.e. $N = 5$ (top left panel), $N = 10$ (top right panel), $N = 20$ (bottom left panel), $N = 40$ (bottom right panel). AL is coloured by magenta, while the rotating lamina is represented by the black solid line. The velocity magnitude is normalized by s.

doi:10.1371/journal.pone.0114687.g009

respectively, as reported in Fig. 11. Notice that the contour plot represents the velocity field. The color legend range is kept fixed in order to highlight the reciprocal difference among the various scenarios. In particular, the higher v, the lower the velocity magnitude is. For sake of completeness, the evolution of the velocity field is depicted in Fig. 12, together with the motion of the immersed individuals, in the scenario characterized by $N = 40$ and $v = 0.1\bar{6}$ at three time instants, i.e. $t = 1\ 000$, $5\ 000$, $13\ 000$, $20\ 000$.

Finally, notice that the author creates a website where the animations showing the velocity field and spatial configuration of the individuals are present (https://www.youtube.com/playlist?list=PL-z4SoMtQxJSHsrIKoZDimokoKf6klFFJ).

The effect of a noise

Previous simulations have been carried out from a deterministic point of view, by neglecting the presence of disorder and disturbance. As known, the dynamics of a group of self-organized individuals can be affected by several random conditions, such as the initial position or the orientation of the individuals. Here, the scenario characterized by $N = 40$ and $v = 0.1\bar{6}$ is employed to dissect the role of a noise. Specifically, at each time step the velocity vector of each individual is rotated by an angle $\phi = \sigma\eta$ where $\sigma = 0.02$ and $\eta \in [0,1]$ is a random number generated by a

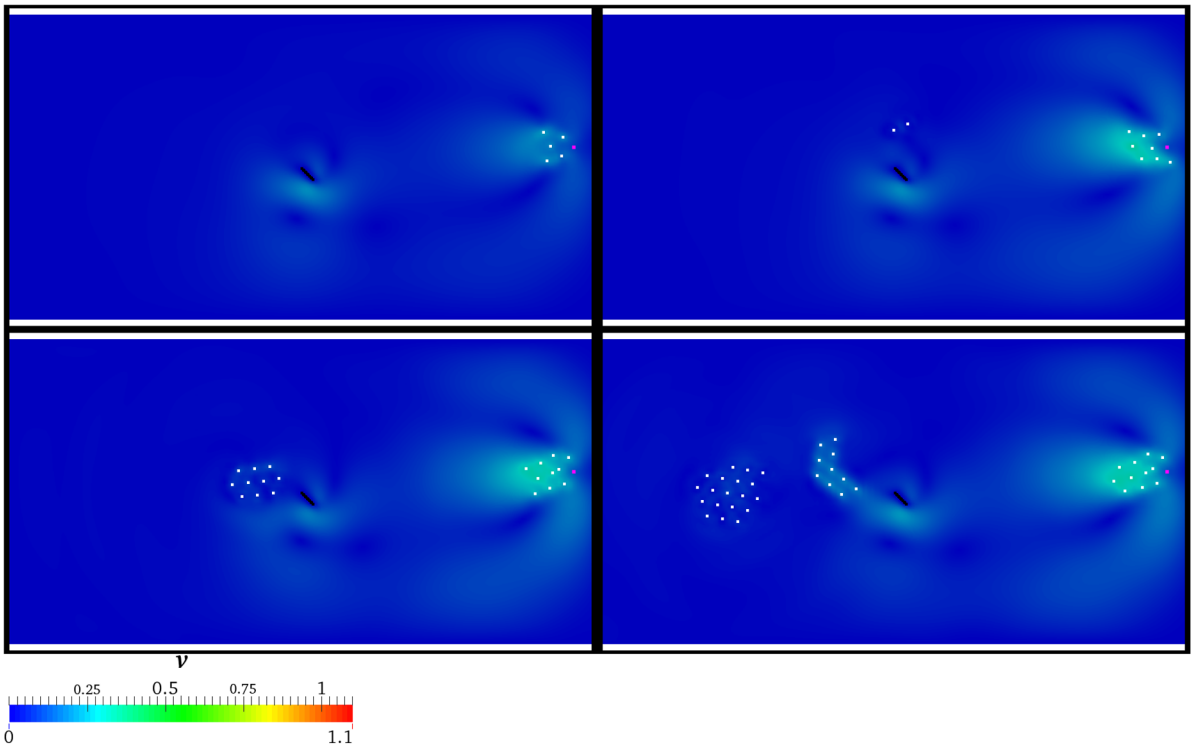

Fig. 10. Presence of the hydrodynamics: $v = 0.08\bar{3}$. Velocity field and spatial configuration of the individuals (white) for different values of N, i.e. $N = 5$ (top left panel), $N = 10$ (top right panel), $N = 20$ (bottom left panel), $N = 40$ (bottom right panel). AL is coloured by magenta, while the rotating lamina is represented by the black solid line. The velocity magnitude is normalized by s.

doi:10.1371/journal.pone.0114687.g010

stochastic process. The author selects the number of individuals following AL at $t = 13\,000$ as a variable to be monitored. A Monte Carlo investigation is performed, consisting of 1 000 simulations. In Fig. 13, the frequency histogram of the monitored quantity is depicted. As it is possible to observe, about the 75% of the simulations leads to a number of followers equal to 11. On the other hand, the remaining part of the simulations affirms that the number of individuals following AL can be 9, 10 or 12, thus achieving a slight mismatch with respect to the more frequent result. In fact, a mean value $\bar{N} = 10.902 \sim 11$ and a variance $\mathrm{var} = 0.382$ are achieved.

Conclusions

In this paper, the collective dynamics of a group of self-organized individuals immersed in a fictitious viscous fluid has been investigated. The group interacts with an additional individual, AL, which aims at becoming a leader. The effect of the fluid forces has been elucidated by combining the LB-IB-TDG strategy for fluid and solid dynamics to the collective behavioural equations. It has been found that the fluid tends to create a more compact group, thus enforcing a deeper exchange of information among the individuals. As a consequence, AL can

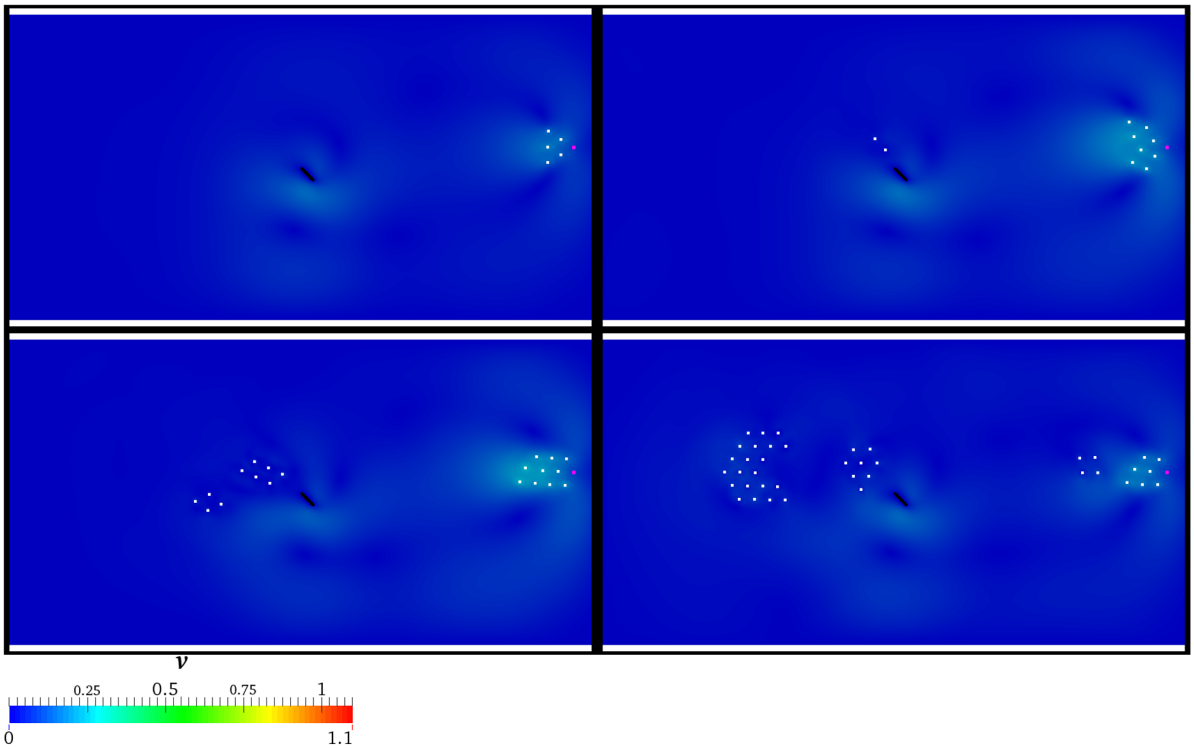

Fig. 11. Presence of the hydrodynamics: $\nu = 0.1\bar{6}$. Velocity field and spatial configuration of the individuals (white) for different values of N, i.e. $N = 5$ (top left panel), $N = 10$ (top right panel), $N = 20$ (bottom left panel), $N = 40$ (bottom right panel). AL is coloured by magenta, while the rotating lamina is represented by the black solid line. The velocity magnitude is normalized by s.

doi:10.1371/journal.pone.0114687.g011

successfully guide the individuals. In addition, groups characterized by progressively larger size have been involved in the computations, showing a splitting effect which increases with N. Present findings lead to assess that the behaviour of the group is considerably affected by the presence of the encompassing fluid. Therefore, an accurate computation of the fluid dynamics is crucial to successfully predict the behaviour of a multi-agent system immersed in a fluid. Notice that the proposed approach represents a substantial improvement with respect to a previous effort carried out by the author [62], where the effects of the hydrodynamics have been investigated for a predator-preys system by using a simple expression for the hydrodynamic force and by neglecting the mass of the individuals. Given the net effect exerted by the fluid, one could conclude that the fluid incidence could be easily incorporate in the purely behavioural equations by increasing the weight of the attraction rule, w_a, thus avoiding the computation of the fluid dynamics. Such approach can lead to wrong predictions about the collective motion. In fact, the fluid dynamics exhibits a strong non-linear dependence on v and the position of the individuals. According to [63], the members which are located in the rear part of the group can benefit from the vortexes characterized by particular wakes created by the front ones, since these experience reduced drag forces. Therefore, an accurate computation of the fluid

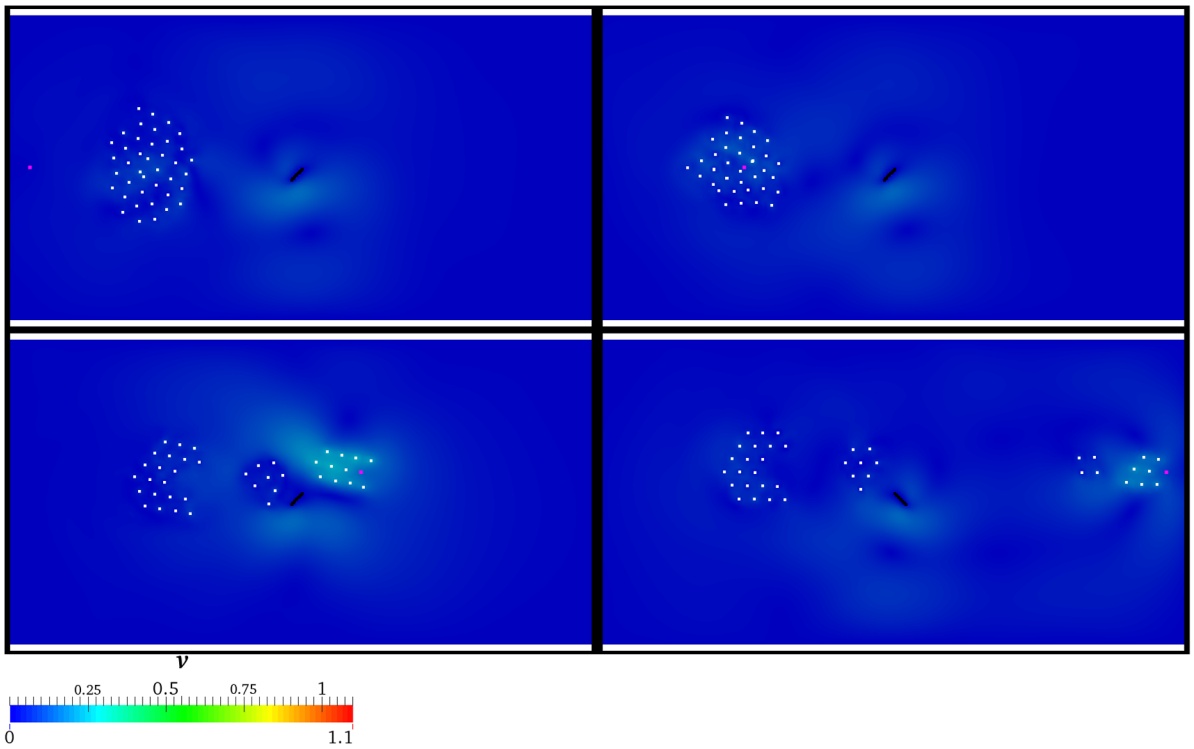

Fig. 12. Velocity field and spatial configuration of the individuals (white) at different time instants, i.e. $t = 1\ 000$ (top left panel), $t = 5\ 000$ (top right panel), $t = 13\ 000$ (bottom left panel), $t = 20\ 000$ (bottom right panel), in the scenario characterized by $v = 0.1\bar{6}$ and $N = 40$. AL is coloured by magenta, while the rotating lamina is represented by the black solid line. The velocity magnitude is normalized by s.

doi:10.1371/journal.pone.0114687.g012

dynamics represents an important aspect to be properly investigated, especially for fish-based studies. Further investigations will dissect the effect of the size of the wake. Specifically, the individuals will be modelled as deformable solid bodies [64, 65] moving in a fluid, aiming at elucidating the incidence of the vorticity field both on the single and collective motions.

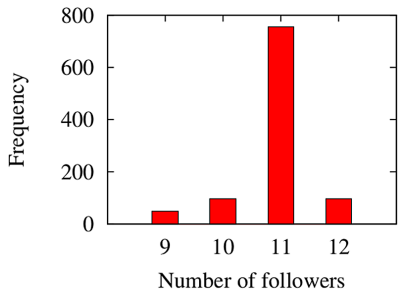

Fig. 13. Frequency histogram of the number of individuals following AL at $t = 13\ 000$. A mean value $\bar{N} = 10.902 \sim 11$ and a variance $\mathrm{var} = 0.382$ are achieved.

doi:10.1371/journal.pone.0114687.g013

Acknowledgments

The author would like to thank Prof. Sauro Succi, Prof. Stefano Ubertini and Prof. Francesco Ubertini for the motivating discussions. The author is also grateful to the editor and the anonymous referees which improved the quality of the present paper with their useful comments.

Author Contributions

Conceived and designed the experiments: AD. Performed the experiments: AD. Analyzed the data: AD. Contributed reagents/materials/analysis tools: AD. Wrote the paper: AD.

References

1. **Lindauer M** (1957) Communication in swarm-bees searching for a new home. Nature 179: 63–66.
2. **Radakov DV** (1973) Schooling in the ecology of fish. New York: J. Wiley.
3. **Krause J, Ruxton GD** (2002) Living in groups. Oxford: Oxford University Press.
4. **Couzin ID, Krause J** (2003) Self-organization and collective behavior in vertebrates. Advances in the Study of Behavior 32.
5. **Vicsek T, Zafeiris A** (2012) Collective motion. Physics Reports 517: 71–140.
6. **Pitcher TJ, Wyche CJ** (1983) Predator-avoidance behaviours of sand-eel schools: why schools seldom split. In: Predators and prey in fishes, Springer. pp. 193–204.
7. **Krause J, Godin JGJ** (1995) Predator preferences for attacking particular prey group sizes: consequences for predator hunting success and prey predation risk. Animal Behaviour 50: 465–473.
8. **Zheng M, Kashimori Y, Hoshino O, Fujita K, Kambara T** (2005) Behavior pattern (innate action) of individuals in fish schools generating efficient collective evasion from predation. Journal of theoretical biology 235: 153–167.
9. **Kunz H, Züblin T, Hemelrijk CK** (2006) On prey grouping and predator confusion in artificial fish schools. In: Proceedings of the Tenth International Conference of Artificial Life. MIT Press, Cambridge, Massachusetts.
10. **Garay J** (2009) Cooperation in defence against a predator. Journal of theoretical biology 257: 45–51.
11. **Ioannou C, Guttal V, Couzin I** (2012) Predatory fish select for coordinated collective motion in virtual prey. Science 337: 1212–1215.
12. **M Jeschke J, Tollrian R** (2005) Effects of predator confusion on functional responses. Oikos 111: 547–555.
13. **Reebs SG** (2000) Can a minority of informed leaders determine the foraging movements of a fish shoal? Animal behaviour 59: 403–409.
14. **Seeley TD** (2003) Consensus building during nest-site selection in honey bee swarms: the expiration of dissent. Behavioral Ecology and Sociobiology 53: 417–424.
15. **Couzin I, Krause J, Franks N, Levin S** (2005) Effective leadership and decision-making in animal groups on the move. Nature 433: 513–516.
16. **Biro D, Sumpter DJ, Meade J, Guilford T** (2006) From compromise to leadership in pigeon homing. Current Biology 16: 2123–2128.
17. **Harcourt JL, Ang TZ, Sweetman G, Johnstone RA, Manica A** (2009) Social feedback and the emergence of leaders and followers. Current Biology 19: 248–252.
18. **King AJ, Johnson DD, Van Vugt M** (2009) The origins and evolution of leadership. Current biology 19: R911–R916.

19. **Abaid N, Bartolini T, Macri S, Porfiri M** (2012) Zebrafish responds differentially to a robotic fish of varying aspect ratio, tail beat frequency, noise, and color. Behavioural Brain Research 233: 545–553.

20. **Polverino G, Porfiri M** (2013) Zebrafish (danio rerio) behavioural response to bioinspired robotic fish and mosquitofish (gambusia affinis). Bioinspiration & Biomimetics 8: 044001.

21. **Marras S, Porfiri M** (2012) Fish and robots swimming together: attraction towards the robot demands biomimetic locomotion. Journal of The Royal Society Interface 9: 1856–1868.

22. **Kopman V, Laut J, Polverino G, Porfiri M** (2013) Closed-loop control of zebrafish response using a bioinspired robotic-fish in a preference test. Journal of the Royal Society Interface 10.

23. **Polverino G, Phamduy P, Porfiri M** (2013) Fish and robots swimming together in a water tunnel: Robot color and tail-beat frequency influence fish behavior. PloS one 8: e77589.

24. **Franks NR, Pratt SC, Mallon EB, Britton NF, Sumpter DJ** (2002) Information flow, opinion polling and collective intelligence in house–hunting social insects. Philosophical Transactions of the Royal Society of London Series B: Biological Sciences 357: 1567–1583.

25. **Ward A, Sumpter D, Couzin I, Hart P, Krause J** (2008) Quorum decision-making facilitates information transfer in fish shoals. Proceedings of the National Academy of Sciences 105: 6948–6953.

26. **Couzin I** (2009) Collective cognition in animal groups. Trends in cognitive sciences 13: 36–43.

27. **Sumpter DJ, Pratt SC** (2009) Quorum responses and consensus decision making. Philosophical Transactions of the Royal Society B: Biological Sciences 364: 743–753.

28. **Leonard NE, Shen T, Nabet B, Scardovi L, Couzin ID, et al.** (2012) Decision versus compromise for animal groups in motion. Proceedings of the National Academy of Sciences 109: 227–232.

29. **Dall SR, Giraldeau LA, Olsson O, McNamara JM, Stephens DW** (2005) Information and its use by animals in evolutionary ecology. Trends in Ecology & Evolution 20: 187–193.

30. **Nabet B, Leonard NE, Couzin ID, Levin SA** (2009) Dynamics of decision making in animal group motion. Journal of nonlinear science 19: 399–435.

31. **Pérez-Escudero A, de Polavieja GG** (2011) Collective animal behavior from bayesian estimation and probability matching. PLoS computational biology 7: e1002282.

32. **Hemelrijk CK, Hildenbrandt H** (2012) Schools of fish and flocks of birds: their shape and internal structure by self-organization. Interface Focus 2: 726–737.

33. **Miller N, Garnier S, Hartnett AT, Couzin ID** (2013) Both information and social cohesion determine collective decisions in animal groups. Proceedings of the National Academy of Sciences 110: 5263–5268.

34. **Kolpas A, Busch M, Li H, Couzin ID, Petzold L, et al.** (2013) How the spatial position of individuals affects their influence on swarms: A numerical comparison of two popular swarm dynamics models. PLoS One 8: e58525.

35. **Couzin I, Krause J, James R, Ruxton G, Franks N** (2002) Collective memory and spatial sorting in animal groups. Journal of Theoretical Biology 218: 1–11.

36. **Hoare D, Couzin I, Godin JG, Krause J** (2004) Context-dependent group size choice in fish. Animal Behaviour 67: 155–164.

37. **Ballerini M, Cabibbo N, Candelier R, Cavagna A, Cisbani E, et al.** (2008) Interaction ruling animal collective behavior depends on topological rather than metric distance: Evidence from a field study. Proceedings of the National Academy of Sciences 105: 1232–1237.

38. **Ballerini M, Cabibbo N, Candelier R, Cavagna A, Cisbani E, et al.** (2008) Empirical investigation of starling flocks: a benchmark study in collective animal behaviour. Animal behaviour 76: 201–215.

39. **Abaid N, Porfiri M** (2010) Fish in a ring: spatio-temporal pattern formation in one-dimensional animal groups. Journal of the Royal Society Interface 7: 1441–1453.

40. **Bode NWF, Franks DW, Wood AJ** (2011) Limited interactions in flocks: relating model simulations to empirical data. Journal of the Royal Society Interface 8: 301–304.

41. **Camperi M, Cavagna A, Giardina I, Parisi G, Silvestri E** (2012) Spatially balanced topological interaction grants optimal cohesion in flocking models. Interface Focus 2: 715–725.

42. **Higuera F, Succi S, Benzi R** (1989) Lattice gas dynamics with enhanced collisions. Europhysics Letters 9: 345–349.

43. **Benzi R, Succi S, Vergassola M** (1992) The lattice Boltzmann equation: theory and applications. Physics Reports 222: 145–197.

44. **Succi S** (2001) The Lattice Boltzmann Equation for Fluid Dynamics and Beyond. Oxford: Clarendon.

45. **Fadlun E, Verzicco R, Orlandi P, Mohd-Yusof J** (2000) Combined immersed-boundary finite-difference methods for three-dimensional complex flow simulations. Journal of Computational Physics 161: 35–60.

46. **Peskin CS** (2002) The immersed boundary method. Acta Numerica 11: 479–517.

47. **Wu J, Shu C** (2009) Implicit velocity correction-based immersed boundary-lattice boltzmann method and its applications. Journal of Computational Physics 228: 1963–1979.

48. **Filippova O, Hänel D** (1997) Lattice Boltzmann simulation of gas-particle flow in filters. Computers & Fluids 26: 697–712.

49. **Mei R, Luo L, Shyy W** (1999) An accurate curved boundary treatment in the lattice Boltzmann method. Journal of Computational Physics 155: 307–330.

50. **Mei R, Yu D, Shyy W, Luo L** (2002) Force evaluation in the lattice Boltzmann method involving curved geometry. Physical Review Letters E 65: 041203.

51. **De Rosis A, Falcucci G, Porfiri M, Ubertini F, Ubertini S** (2014) Hydroelastic analysis of hull slamming coupling lattice Boltzmann and finite element methods. Computers & Structures 138: 24–35.

52. **De Rosis A, Ubertini S, Ubertini F** (2014) A comparison between the interpolated bounce-back scheme and the immersed boundary method to treat solid boundary conditions for laminar flows in the lattice boltzmann framework. Journal of Scientific Computing.

53. **De Rosis A, Ubertini S, Ubertini F** (2014) A partitioned approach for two-dimensional fluid-structure interaction problems by a coupled lattice Boltzmann-finite element method with immersed boundary. Journal of Fluids and Structures 45: 202–215.

54. **De Rosis A, Falcucci G, Ubertini S, Ubertini F** (2014) Aeroelastic study of flexible flapping wings by a coupled lattice Boltzmannfinite element approach with immersed boundary method. Journal of Fluids and Structures 49: 516–533.

55. **De Rosis A** (2014) On the dynamics of a tandem of asynchronous flapping wings: Lattice boltzmann-immersed boundary simulations. Physica A: Statistical Mechanics and its Applications 410: 276–286.

56. **De Rosis A** (2014) A lattice Boltzmann-finite element model for two-dimensional fluid-structure interaction problems involving shallow waters. Advances in Water Resources 65: 18–24.

57. **De Rosis A** (2014) A lattice Boltzmann model for multiphase flows interacting with deformable bodies. Advances in Water Resources 73: 55–64.

58. **De Rosis A** (2014) Harmonic oscillations of laminae in non-Newtonian fluids: A lattice Boltzmann-immersed boundary approach. Advances in Water Resources 73: 97–107.

59. **Mancuso M, Ubertini F** (2003) An efficient integration procedure for linear dynamics based on a Time Discontinuous Galerkin formulation. Computational Mechanics 32: 154–168.

60. **Mancuso M, Ubertini F** (2006) An efficient Time Discontinuous Galerkin procedure for non-linear structural dynamics. Computer Methods in Applied Mechanics and Engineering 195: 6391–6406.

61. **Bhatnagar P, Gross E, Krook M** (1954) A model for collision processes in gases. I. Small amplitude processes in charged and neutral one-component systems. Physical Review 94: 511–525.

62. **De Rosis A** (2014) Hydrodynamic effects on a predator approaching a group of preys. Physica A: Statistical Mechanics and its Applications 414: 329–339.

63. **Hemelrijk C, Reid D, Hildenbrandt H, Padding J** (2014) The increased efficiency of fish swimming in a school. Fish and Fisheries: n/a–n/a.

64. **Felippa C, Haugen B** (2005) A unified formulation of small-strain corotational finite elements: I. Theory. Computer Methods in Applied Mechanics and Engineering 194: 2285–2335.

65. **Garcea G, Madeo A, Zagari G, Casciaro R** (2009) Asymptotic post-buckling fem analysis using corotational formulation. International Journal of Solids and Structures 46: 377–397.